Journal of Power Sources 198 (2012) 42–50

Contents lists available at SciVerse ScienceDirect

Journal of Power Sources

journal homepage: www.elsevier.com/locate/jpowsour

Effects of residual oxygen partial pressure on the degradation of polymer electrolyte membrane fuel cells under reverse current conditions

KwangSup Eom[a], Yoo Yeon Jo[a], EunAe Cho[a,*], Tae-Hoon Lim[a], Jong Hyun Jang[a], Hyoung-Juhn Kim[a], Bo Ki Hong[b], Jong Hyun Lee[b]

[a] Fuel Cell Center, Korea Institute of Science and Technology (KIST), Seoul 136-791, Republic of Korea
[b] Fuel Cell Vehicle Team 1, Eco-Technology Center, Hyundai-Kia Motors, 104 Mabuk-Dong, Giheung-Gu, Yongin-Si, Gueonggi-Do 446-912, Republic of Korea

ARTICLE INFO

Article history:
Received 4 August 2011
Received in revised form
20 September 2011
Accepted 23 September 2011
Available online 1 October 2011

Keywords:
Polymer electrolyte membrane fuel cell
Degradation
Durability
Reverse current condition
Oxygen partial pressure

ABSTRACT

A PEMFC stack inevitably experiences reverse current conditions during startup and shutdown processes. Residual oxygen partial pressure in the stack affects the local potential in the cathode facing oxygen in the anode and plays a critical role in cathode degradation. In this study, effects of residual oxygen partial pressure on PEMFC degradation were studied under reverse current conditions. Increasing the residual oxygen partial pressure under repetitive reverse current conditions accelerates performance decay and facilitates cathode degradation. Cathode degradation is revealed by an increase in charge-transfer resistance and a decrease in electrochemical active surface area, which can be attributed to corrosion of the carbon support and dissolution/migration and agglomeration of the platinum catalyst.

1. Introduction

Polymer electrolyte membrane fuel cells (PEMFCs) are attractive alternative power sources for next-generation vehicles due to their safe emission, high conversion efficiency, and high energy density [1–3]. One of the critical issues in commercializing fuel cell vehicles is the durability and cost of the PEMFC stack [4]. To reach the United States Department of Energy's durability target for commercialization (a 5000 h lifetime), many efforts have been devoted to the development of durable materials for PEMFC stacks [5], including catalysts [6], supports [7–9], membranes, and bipolar plates, and to the development of durable operating techniques [10–12]. Although it is very difficult to clearly define the lifetime of an automotive PEMFC stack, it is generally accepted that current technology cannot reach the target lifespan of 5000 h under dynamic operating conditions including startup–shutdown, freeze–thaw, and humid-dry cycles [5]. Particularly, startup–shutdown cycles that induce the so-called reverse current condition are known to result in membrane-electrode assembly (MEA) degradation by causing carbon corrosion [7–9] and platinum dissolution/oxidation/agglomeration [10–12].

Fig. 1(a) schematically illustrates a representative formation of the reverse current condition in a PEMFC stack [10]. During operation, anode and cathode gas channels are filled with hydrogen and air, respectively (Stage 1). To shutdown the stack, the electrical load (power output) is turned off, the air supply is stopped, and a dummy load is connected between the anode and cathode to remove oxygen from the cathode gas channel (Stage 2). When the oxygen in the cathode gas channel is completely consumed, the hydrogen supply is stopped. After that, the stack is left alone while the vehicle is parked. Then, ambient air diffuses into the stack through the air exhaust vent and crosses over through the membrane to the anode gas channel (Stage 3). Oxygen from ambient air reacts with residual hydrogen, and eventually the anode and cathode gas channels are filled up with $N_2 + xO_2$ gas (Stage 4, $x = 0$–21%). As storage time goes on, oxygen partial pressure in the gas channels increases up to 21% (air). To start up the stack, the dummy load is disconnected, and hydrogen and air are fed into the anode and cathode gas channels, respectively. The reverse current condition occurs when a hydrogen/oxygen boundary forms in the anode gas channel while oxygen is present in the cathode gas channel (Stage 5). Under these conditions, as shown in Fig. 1(b), a potential that is up to twice as high as the open circuit voltage (OCV) is locally present in the cathode (D) facing oxygen in the anode gas channel (B) [5–9]. Under reverse current conditions, cathode degradation occurs mainly due to the oxidation of carbon and platinum, as follows [8]:

$$C + 2H_2O \rightarrow CO_2 + 4H^+ + 4e^- \quad (1a)$$

$$C + O_2 \rightarrow CO_2 \quad (1b)$$

* Corresponding author. Tel.: +82 2958 5279; fax: +82 2958 5199.
E-mail address: eacho@kist.re.kr (E. Cho).

0378-7753/$ – see front matter © 2011 Elsevier B.V. All rights reserved.
doi:10.1016/j.jpowsour.2011.09.085

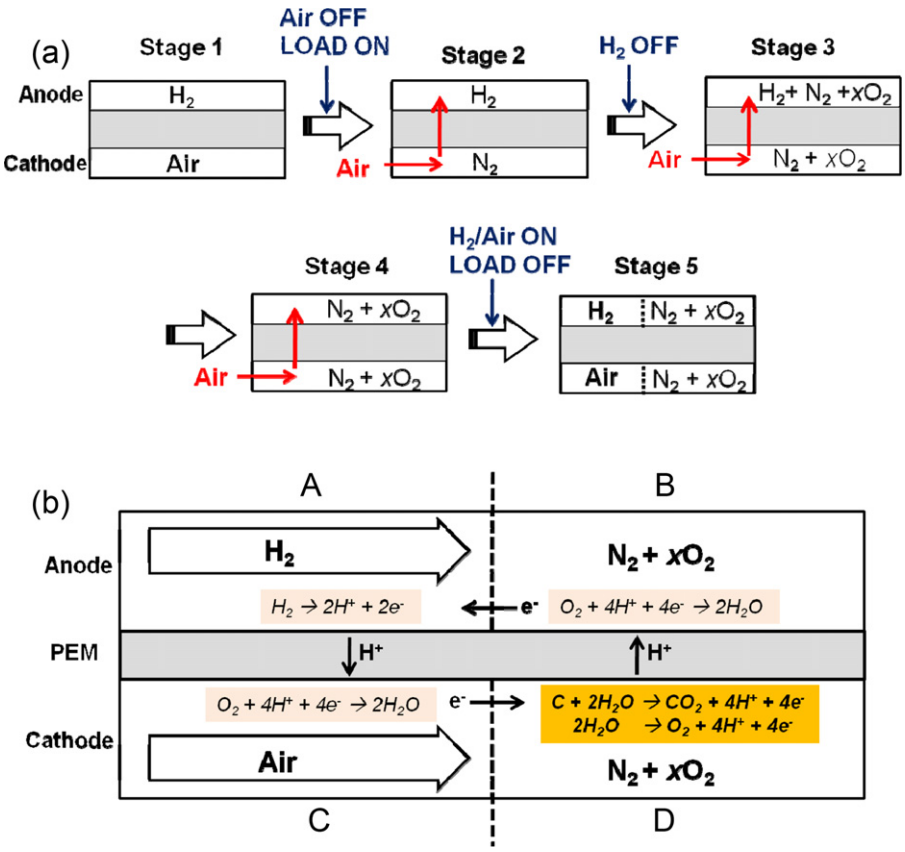

Fig. 1. (a) A schematic showing formation of reverse current conditions during shutdown–startup process and (b) the mechanism of reverse-current reactions, induced in Stage 5 [5,6].

$$Pt + xH_2O \rightarrow PtOx + 2xH^+ + 2xe^- \quad (2a)$$

$$Pt + xO_2 \rightarrow PtO_{2x} \quad (2b)$$

In the previous studies [11,12], we found that under the repetitive reverse current condition, cathode degraded more severely at higher cell temperature (40–80 °C) upon more humid reactant gases (RH 0–100%) due to faster oxidation reaction rate of carbon and platinum described in Eqs. (1) and (2). From Eqs. (1b) and (2b), oxygen concentration as well as water content in cathode was expected to affect the cathode degradation rate.

As a new approach to mitigate cathode degradation caused by reverse current conditions, we focused on the residual oxygen partial pressure in the gas channels upon startup. The potential present in region D in Fig. 1(b) increases with the residual oxygen partial pressure in regions B and D according to the well-known Nernst equation [13]. Thus, higher residual oxygen partial pressure results in faster electrochemical and chemical oxidation of carbon and platinum as given in Eqs. (1) and (2). Therefore, it is expected that suppressing diffusion of ambient air into the stack and keeping the residual oxygen partial pressure low will reduce cathode degradation. In this study, we investigated the effects of residual oxygen partial pressure in the gas channels on degradation of PEMFCs under reverse current conditions.

2. Experimental methods

2.1. Single cell preparation and operation

Single cells were prepared with a commercial membrane electrode assembly (MEA) with an active area of 25 cm^2, SGL GDLs, and graphite bipolar plates (BPs) with serpentine flow fields. Assembled single cells were operated at 65 °C using hydrogen and air with RH of 100%, followed by activation at 0.4 V for 24 h. The stoichiometry ratios (SRs) of fuel (H_2) and oxidant (air) were 1.5 and 2.0, respectively.

2.2. Startup–shutdown cycling test

Fig. 2 shows a schematic voltage profile for the startup–shutdown cycle employed in this study [10–12,14–17]. As an operating step, hydrogen and air were supplied to the anode and the

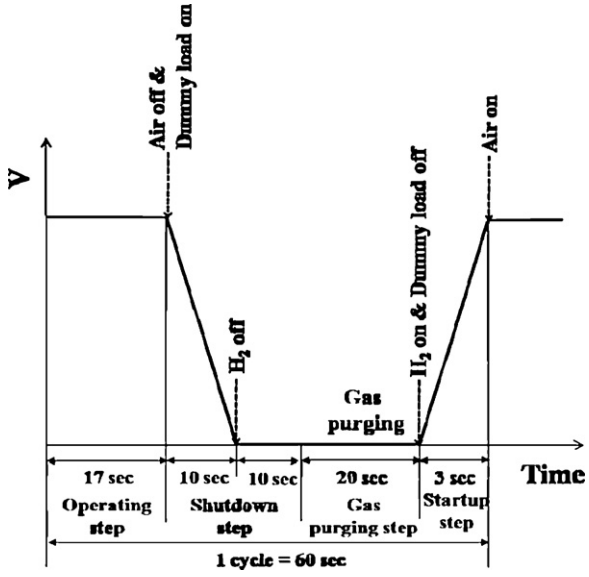

Fig. 2. Experimental load profile for the startup–shutdown cycle employed in this study.

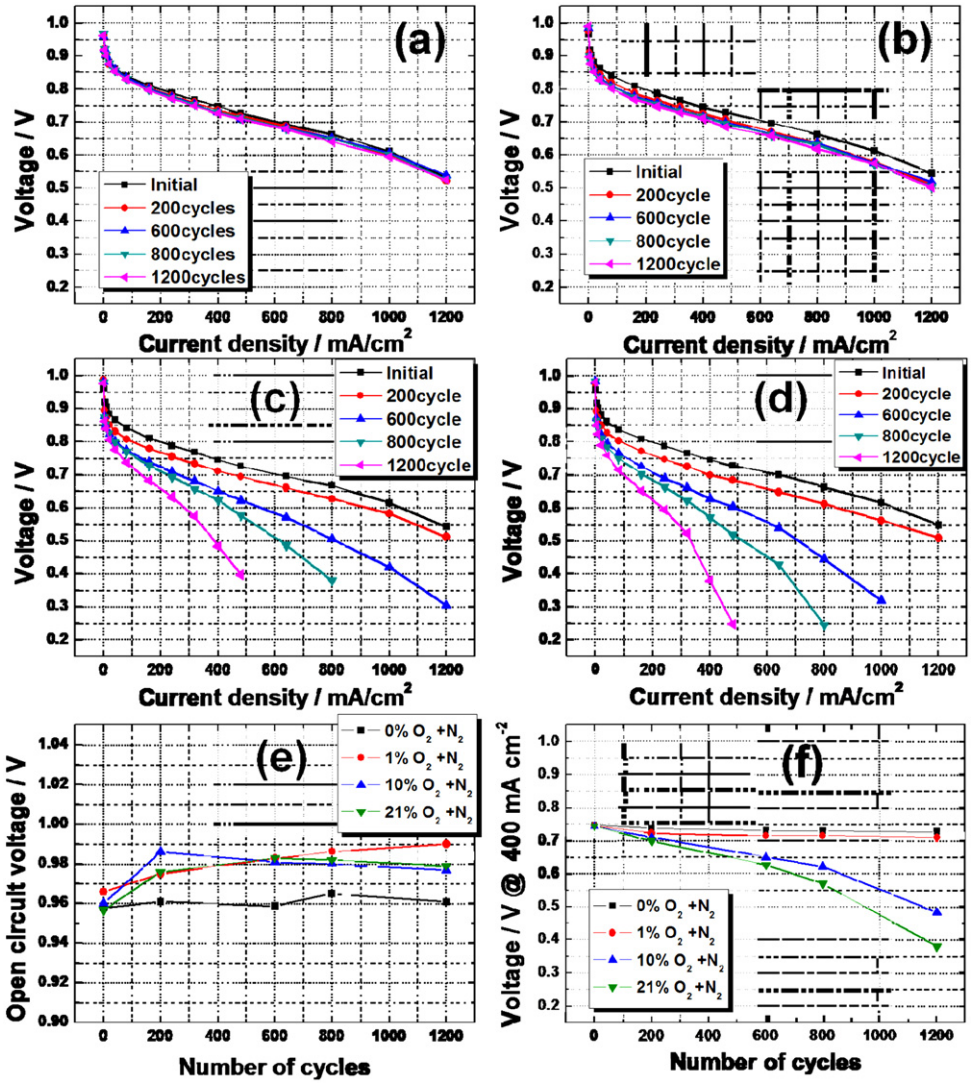

Fig. 3. Effects of oxygen concentration in the purging gas ($N_2 + xO_2$) on *i–V* curves for the single cells during 1200 startup–shutdown cycles: x = (a) 0, (b) 1, (c) 10, and (d) 21%. (e) OCV and (f) cell voltage at 400 mA cm^{-2} as a function of the number of cycles.

cathode, respectively, for 17 s (Stage 1 in Fig. 1(a)). Upon shutdown, the air supply was stopped and a dummy load was connected between the anode and the cathode to remove oxygen from the cathode (Stage 2 in Fig. 1(a)). In 10 s, hydrogen supply was stopped and kept for another 10 s. Because the complete consumption of hydrogen in the anode by reaction with oxygen from natural diffusion is slow, and because it is difficult to monitor and control the residual oxygen partial pressure, the anode and cathode gas channels were purged with a mixture of $N_2 + xO_2$ (x = 0, 1, 10, 21%) gas for 20 s to simulate stage 4 in Fig. 1(a). Then, to startup the single cell, hydrogen was supplied to the anode while the dummy load was disconnected, and in 3 s, air was fed to the cathode (Stage 5 in Fig. 1(a)).

During the startup–shutdown cycles, cell temperature was 65 °C, and the RH of all the gases was 100%. The flow rates of hydrogen and $N_2 + xO_2$ mixture gas were determined so that the SR of hydrogen and oxygen were 1.5 or 2.0 at a given current density of 800 mA cm^{-2}.

2.3. Electrochemical characterizations of the single cells

To characterize the electrochemical properties of the single cells, current density–voltage (*i–V*), electrochemical impedance spectroscopy (EIS), cyclic voltammetry (CV), and linear sweep voltammetry (LSV) were performed. EIS was measured from 50 mHz and 10 kHz. The amplitude of the sinusoidal current signal was 5 mV at an applied potential of 0.85 V. The anode served as both reference and counter electrode, and the cathode was employed as the working electrode. We assumed that reactions at the anode were negligible [18]. CV was measured from 50 mV to 1.2 V at a scan rate of 50 mV s^{-1}. LSV was measured in the voltage range from 0 to 0.6 V at a scan rate of 2 mV s^{-1}. When CV and LSV were measured, humidified N_2 gas was fed to the cathode. CV and LSV were used to measure the electrochemically active surface area (EAS) of the cathode and the hydrogen gas crossover rate (from anode to cathode) through the membrane, respectively.

2.4. Post-mortem analyses of MEA

Cross-sectional images of MEAs were measured by scanning electron microscopy (SEM). The surface compositions of the MEAs were analyzed by wavelength dispersive spectroscopy (WDS). Distribution of Pt species on cross-sectional MEA was observed using electron probe X-ray microanalysis (EPMA). The particle size of Pt catalyst was obtained from transmission electron microscopy (TEM). To analyze the chemical bond structure of the

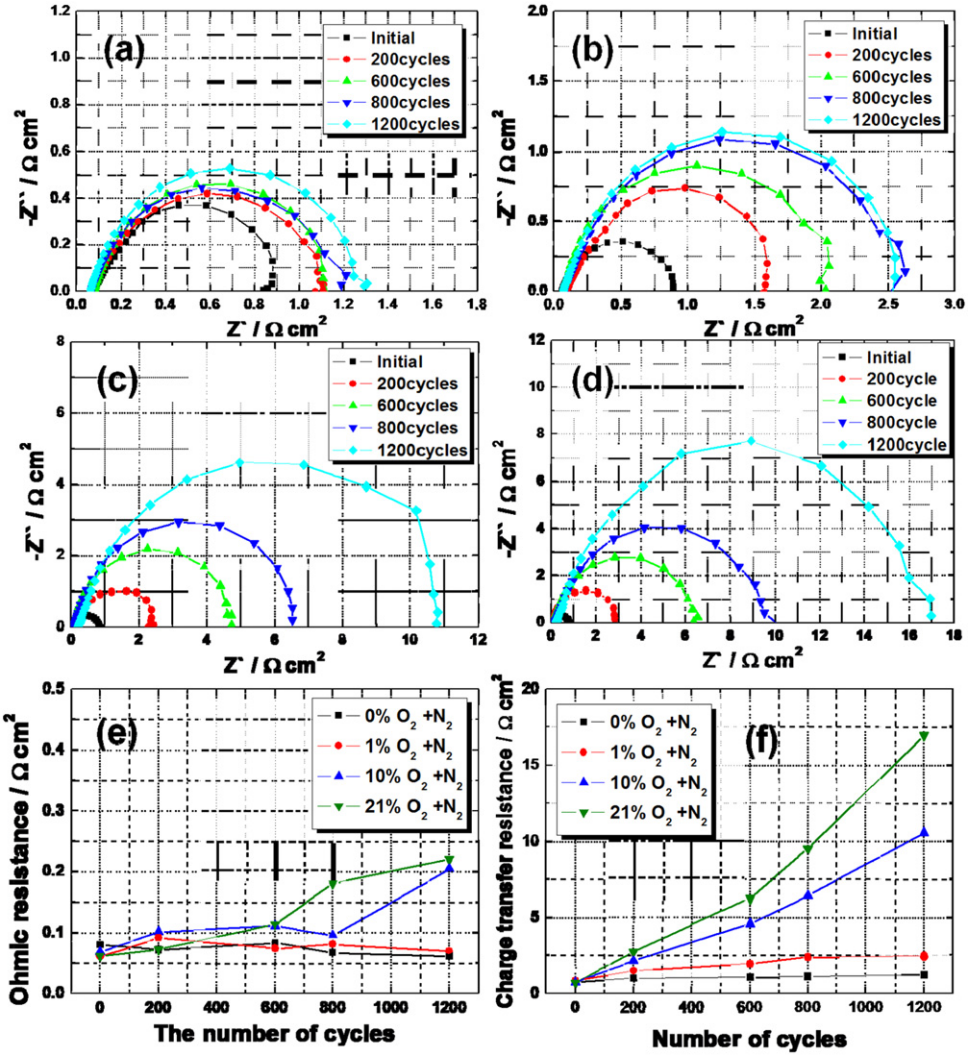

Fig. 4. Effects of oxygen concentration in the purging gas ($N_2 + xO_2$) on Nyquist plots for the single cells during 1200 startup–shutdown cycles: x = (a) 0, (b) 1, (c) 10, and (d) 21%. (e) R_{oh} and (f) R_{ct} as a function of the number of cycles.

membranes, Fourier transform infrared spectroscopy (FT-IR) was employed.

3. Results and discussion

3.1. Degradation of cell performance

Fig. 3(a)–(d) shows current density–voltage (i–V) curves for the single cells measured before and after 200, 600, 800, and 1200 cycles employing a mixture of $N_2 + xO_2$ gas (x = 0, 1, 10, and 21%), as described in Fig. 2. With 0 or 1% O_2 gas, performance decay was barely observed during 1200 cycles, while with 10 or 21% O_2 gas, cell performance decreased dramatically with repeated cycling. From the data in Fig. 3(a)–(d), the open circuit voltage (OCV) and the voltage at a current density of 400 mA cm^{-2} for a single cell were plotted as a function of cycle number in Fig. 3(e) and (f), respectively. Fig. 3(e) shows that the OCV value changed slightly, from 0.96 to 0.99 V over 1200 cycles, reflecting that gas crossover through the membrane was not strongly affected by the startup–shutdown cycles for all of the gas mixtures [11]. On the other hand, the cell voltage at a current density of 400 mA cm^{-2} decreased with the cycle number, as presented in Fig. 3(f). For the cycles with 0 or 1% O_2 gas, cell voltage decreased very slowly during 1200 cycles, from 0.75 to 0.73 V, and from 0.75 to 0.71 V, respectively. In contrast, for the cells with 10 or 21% O_2 gas, cell voltage decreased drastically from 0.74 to 0.48 V and 0.38 V, respectively. Voltage decay rate was calculated to be 17, 33, 210, and 300 μV/cycle for the cycles with 0, 1, 10, and 21% $O_2 + N_2$ gas. These results show that with repetitive formation of reverse current conditions, cell performance decayed faster with higher residual oxygen partial pressure in the gas channel. With increasing oxygen partial pressure, the equilibrium potential of hydrogen oxidation–oxygen reduction cell increases as follows:

$$E = \frac{-\Delta G(T)}{2F} + \frac{RT}{2F} \ln \frac{p_{H_2} \cdot p_{O_2}^{0.5}}{p_{H_2O}} \quad (3)$$

In Eq. (3), E is the reversible cell voltage (V), $\Delta G(T)$ is the Gibbs free energy change during a fuel cell reaction (J mol^{-1}), F is Faraday's constant (96,485 C mol^{-1}), R is the ideal gas constant (8.314 J mol^{-1} K^{-1}), and T is the temperature (K). Eq. (2) becomes the well-known Nernst equation [13] when the activities of the reactant and product are replaced by the partial gas pressure (p).

Thus, the potential present in region D in Fig. 1(b), which is twice the OCV, increases with oxygen partial pressure, resulting in faster electrochemical oxidation of carbon and platinum as described in Eqs. (1a) and (2a). In addition, the chemical oxidation of carbon and platinum, described in Eqs. (1b) and (2b), will also occur faster with higher oxygen partial pressure. Therefore,

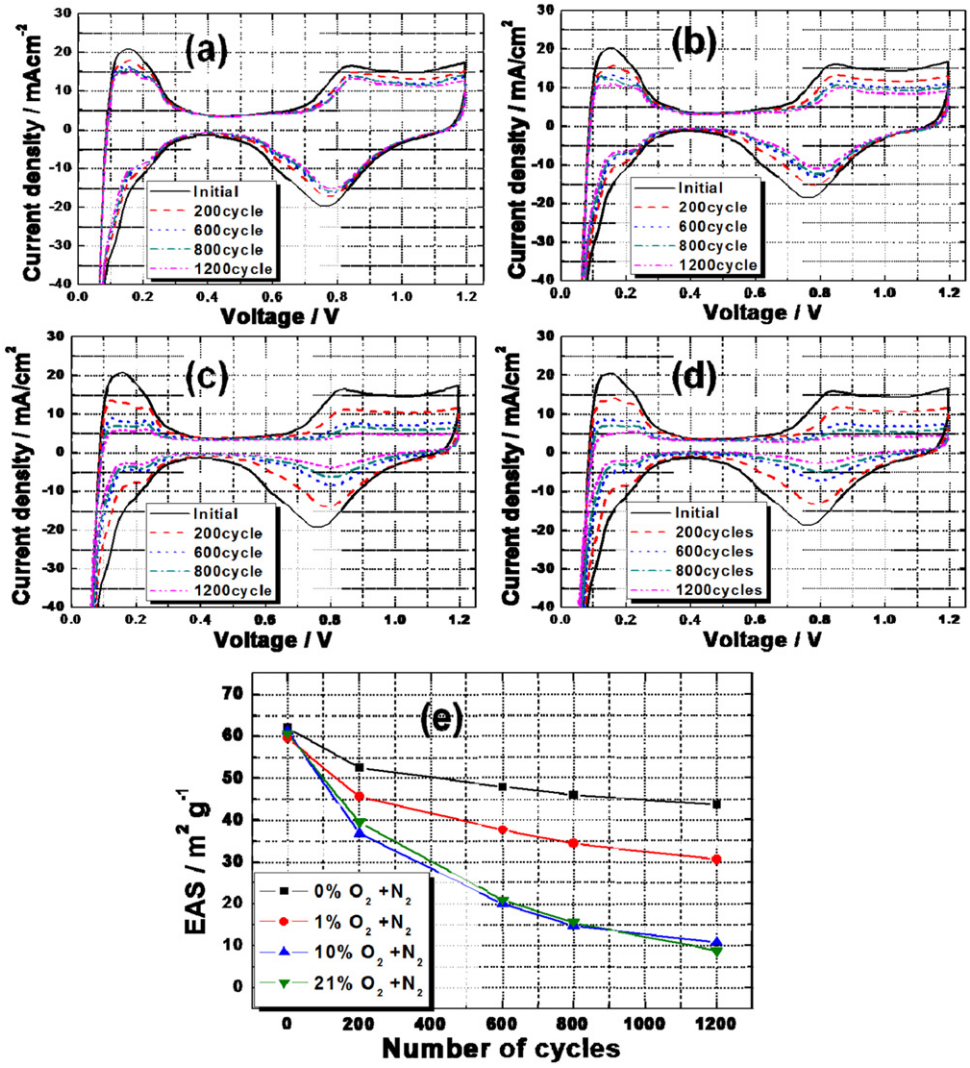

Fig. 5. Effects of oxygen concentration in the purging gas ($N_2 + xO_2$) on cyclic voltammograms for single cells during 1200 startup–shutdown cycles: x = (a) 0, (b) 1, (c) 10, and (d) 21%. (e) EAS as a function of the number of cycles.

cathode degradation that is attributed to the oxidation of carbon and platinum will be accelerated with higher residual oxygen partial pressure under reverse current conditions.

3.2. Electrochemical analyses

To examine the effects of residual oxygen partial pressure on the electrochemical properties of the single cells experiencing repetitive reverse current conditions, electrochemical impedance spectroscopy (EIS), cyclic voltammetry (CV), and linear sweep voltammetry (LSV) were performed before and after 200, 600, 800, 1200 cycles employing $N_2 + xO_2$ mixture gas (x = 0, 1, 10, and 21%) as described in Fig. 2.

Fig. 4(a)–(d) present Nyquist plots for the single cells obtained from EIS. A standard semicircle was obtained for all experimental cases. The high-frequency intersection of the x-axis frequency and the diameter of the semicircle correspond to the ohmic resistance (R_{ohm}) and charge-transfer resistance (R_{ct}), respectively. From the data in Fig. 4(a)–(d), R_{ohm} and R_{ct} were plotted versus cycle number in Fig. 4(e). During 1200 cycles, R_{ohm} remained almost at a constant value of 0.06 Ω cm^2 for cells cycled with N_2 + 0 or 1% O_2 gas. In contrast, R_{ohm} increased from 0.06 to 0.21 and 0.22 Ω cm^2 for cells cycled with N_2 + 10 or 20% O_2 gas, respectively. This increase is associated with a decrease in the ionic conductivity of the membrane or in the electronic conductivity of the electrodes. As will be discussed below, the increase in R_{ohm} is more likely caused by a decrease in the electronic conductivity of the cathode resulting from corrosion of the carbon support than by a decrease in ionic conductivity of the membrane. During 1200 cycles with N_2 + 0, 1, 10 and 21% O_2 gas, R_{ct} of the single cells increased from 0.76 to 1.2, 2.5, 10.6 and 17.0 Ω cm^2, respectively, in a good agreement with the performance decay shown in Fig. 3.

To evaluate electrochemical active surface area (EAS), CV was performed, and the results are presented in Fig. 5(a)–(d). From the hydrogen desorption peak observed at about 100 mV, EAS was calculated under the assumption that the normalized charge density for a monolayer of adsorbed hydrogen on polycrystalline platinum is 210 μC cm^{-2} [19]; the calculations of EAS are summarized in Fig. 5(e). Pt loading for the cathode was 0.4 mg cm^{-2}. With repeated cycling, EAS decreased for all the cells, from 60–62 to 44, 31, 11 and 8.9 m^2 g^{-1} for O_2 concentrations of 0, 1, 10 and 21%. The decrease in EAS may be caused by loss and/or agglomeration of Pt catalyst in the cathode.

Hydrogen crossover current density obtained from LSV (not shown here) remained almost constant at 1.6 mA cm^{-2} during the 1200 cycles irrespective of oxygen partial pressure, implying that physical degradation of the membrane such as thinning and pinhole formation was negligible.

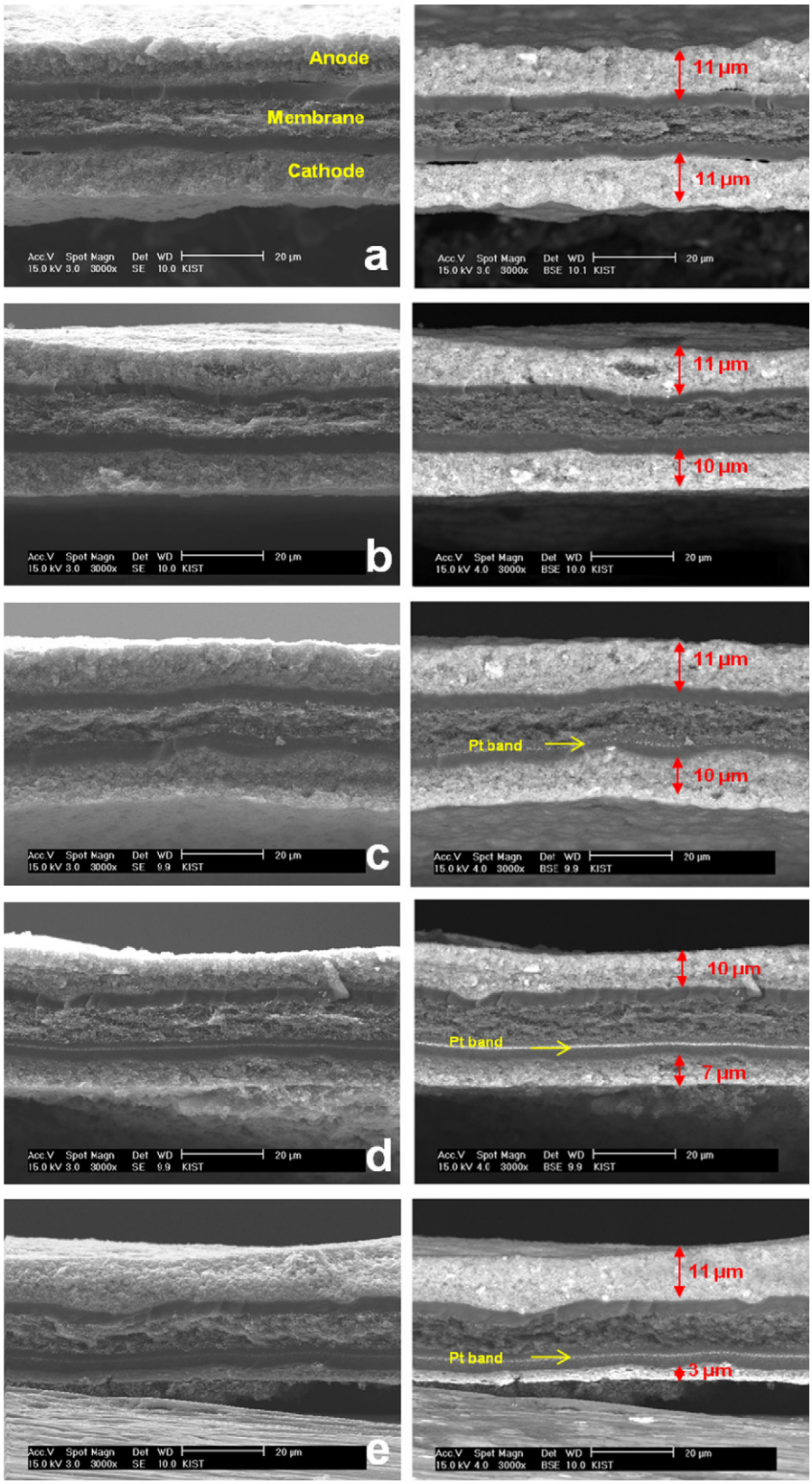

Fig. 6. Cross-sectional SEM images for the MEAs (a) before and after 1200 startup–shutdown cycles employing (b) 0, (c) 1, (d) 10, and (e) 21% O_2 in the purging gas ($N_2 + xO_2$).

3.3. Post-mortem analyses of MEA

To investigate the physical and chemical degradation of the MEAs after the startup–shutdown cycles employing $N_2 + xO_2$ mixture gas ($x = 0$, 1, 10, and 21%), after 1200 cycles, the cycled MEAs were analyzed by SEM, WDS, EPMA, TEM, and FTIR and compared with a fresh MEA. Fig. 6 exhibits cross-sectional SEM images for the MEAs. The anode and membrane thickness remained 11

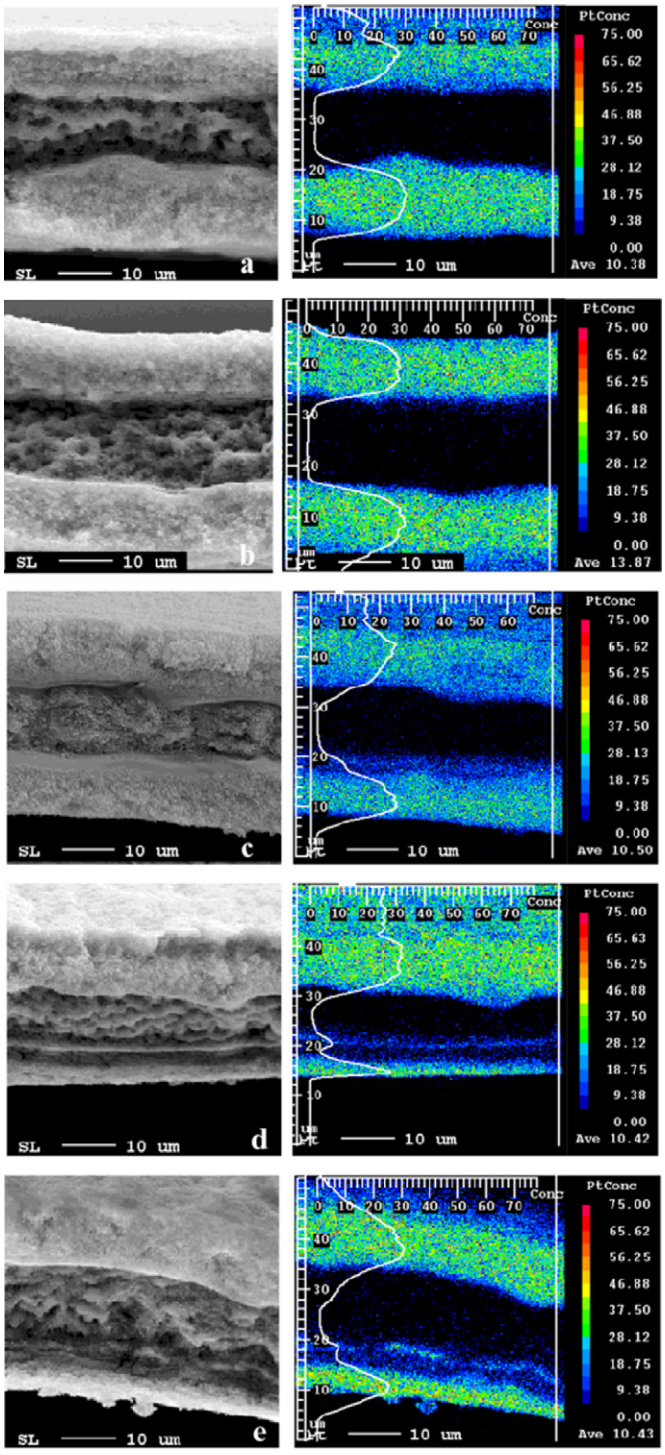

Fig. 7. Cross-sectional BSEM (left) and EPMA (right, mapped for Pt) images for the MEAs (a) before and after 1200 startup–shutdown cycles employing (b) 0, (c) 1, (d) 10, and (e) 21% O_2 in the purging gas ($N_2 + xO_2$).

and 20 μm, respectively, before and after cycling, irrespective of residual oxygen partial pressure. In contrast, cathode thickness decreased remarkably with higher oxygen concentration, from 11 to 11, 10, 7 and 3 μm with 0, 1, 10, and 21% O_2 gas. This decrease shows that increasing residual oxygen partial pressure facilitated carbon corrosion in the cathode.

Increasing the cathode potential and oxygen concentration in the cathode gas channel should increase Pt catalyst oxidation as well as carbon corrosion. As shown in Fig. 6, a Pt band was observed

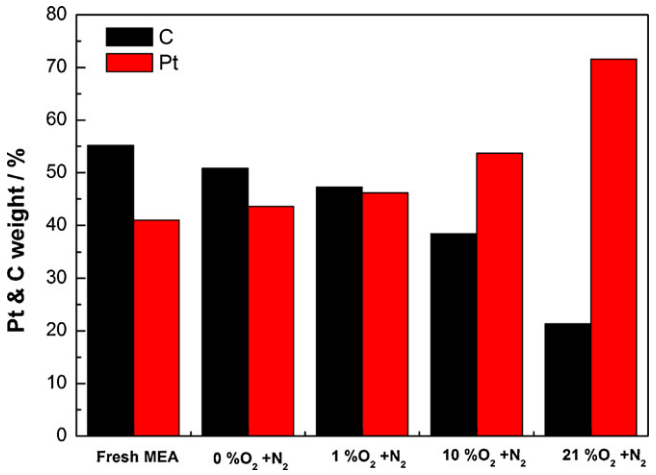

Fig. 8. Chemical composition of the cathode before and after the 1200 startup–shutdown cycles using the purging gas ($N_2 + xO_2$).

Table 1
Average sizes of Pt particles measured by image analysis of the bright-filed TEM images (Fig. 9) before and after cycles employing various oxygen partial pressures ((a) 0%, (b) 1%, (c) 10%, and (d) 21% O_2) in purging gases.

Samples	Anode (nm)	Cathode (nm)
Before cycling	2.46	2.34
N_2 (0% O_2)	2.77	3.47
1% O_2	2.81	3.32
10% O_2	3.04	4.96
Air (21% O_2)	3.14	5.25

in the membrane. To confirm the migration of Pt into the membrane, EPMA mapping images for Pt were obtained as shown in Fig. 7. Even though it is difficult to estimate the amount of Pt in the membrane quantitatively, Fig. 6 suggests that more Pt migrated into the membrane with increasing residual oxygen partial pressure. Previous studies reported that a Pt band line in the membrane may be formed by dissolved Pt species diffusing from the cathode and precipitating in the membrane by reduction with crossover hydrogen from the anode [20–22].

As discussed above, carbon corrosion and Pt oxidation and migration occurred simultaneously in the cathode under reverse current conditions. To estimate the relative loss of carbon and Pt, the chemical composition of the cathode was measured, and the weight percent of carbon and Pt were plotted, as shown in Fig. 8. For a fresh MEA, the weight percent ratio of carbon to Pt was 55:41 (the remaining 4% was fluorine). After 1200 cycles, carbon to Pt was 51:44, 47:46, 38:54, and 21:72 for the single cells operated with 0, 1, 10, and 21% $O_2 + N_2$ mixture gas. In other words, higher residual oxygen partial pressure caused a faster loss of carbon from the cathode compared to Pt.

To investigate the effects of oxygen concentration on any growth of Pt catalyst particles, TEM images were obtained. Fig. 9 shows clearly the growth of Pt particles, particularly for the cathode cycled with higher oxygen concentration gas. The calculated Pt particle

Table 2
Selected infrared absorption bands of H-Nafion [23].

Band location (cm^{-1})	Assignment
~960 strong	C–O–C stretching, symmetric
~980 strong	C–F stretching (–CF_2–CF(CF_3)-group)
~1060 strong	S–O stretching, symmetric
~1100 very strong, very broad	CF_2 stretching, symmetric
~1200 very strong, very broad	CF_2 stretching, asymmetric

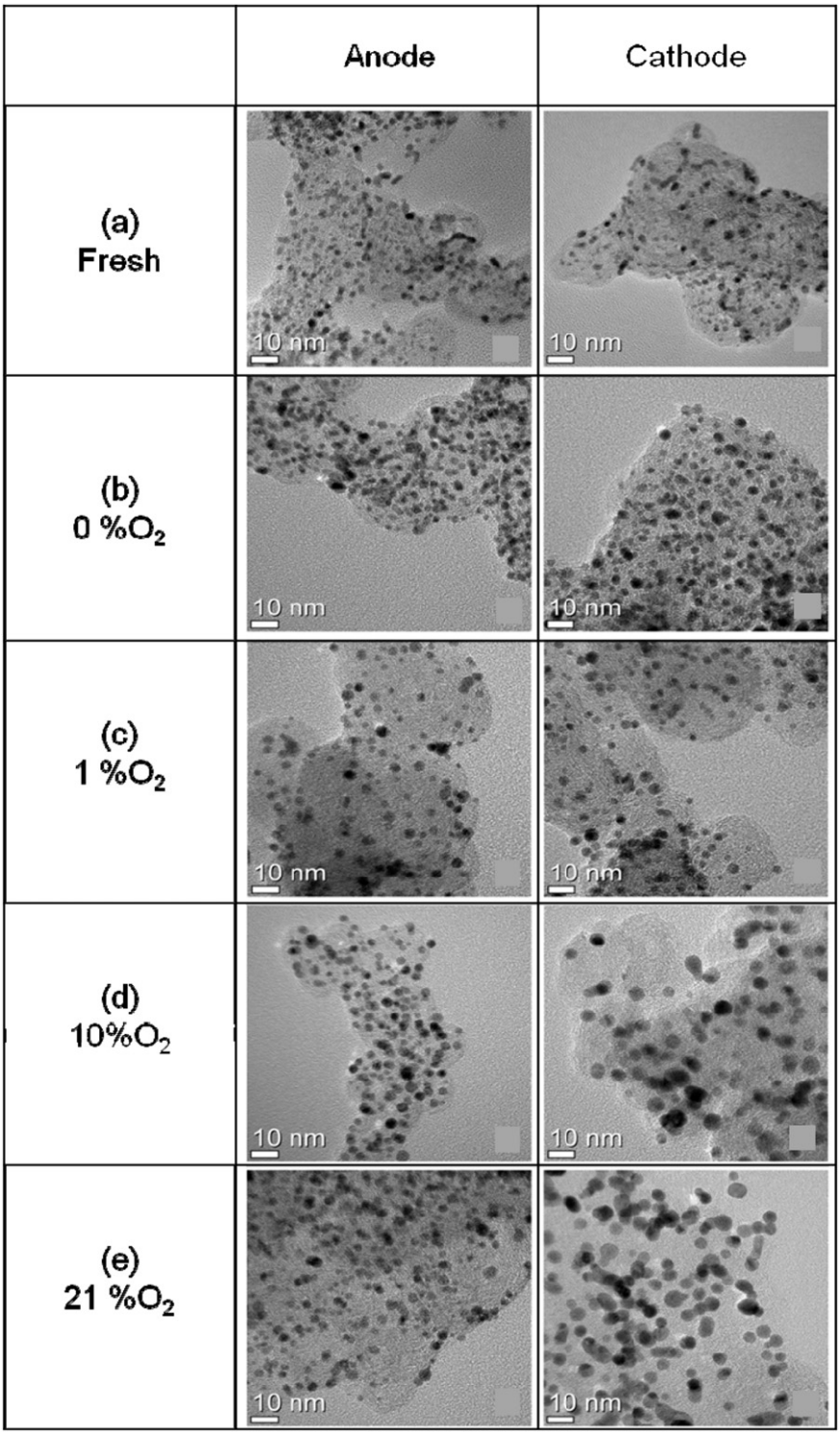

Fig. 9. TEM images for the anode (left) and cathode (right) catalyst (a) before and after 1200 startup–shutdown cycles employing (b) 0, (c) 1, (d) 10, and (e) 21% O_2 in the purging gas ($N_2 + xO_2$).

size is summarized in Table 1. For the anode, the Pt particle size increased slightly from 2.46 to 2.77, 2.81, 3.04 and 3.14 nm for 0, 1, 10, and 21% $O_2 + N_2$ mixture gas. For the cathode, the Pt particle size increased from 2.34 to 3.47, 3.32, 4.96 and 5.25 nm. These results reflect that increasing the residual oxygen partial pressure increases the potential at the cathode and facilitates carbon corrosion and Pt dissolution/agglomeration. These reactions result in an increase in R_{ct} and a decrease in EAS, which, in turn, lead to a decay in cell performance.

To examine the degradation of the membrane, the chemical structure of the membranes was analyzed by FT-IR before and after cycling, as shown in Fig. 10. Table 2 summarizes the well-assigned vibrational bands, based on previously published data [23]: C–F stretching (–CF_2–CF(CF_3)-group) at 980 cm^{-1}, S–O symmetric stretching at 1060 cm^{-1}, CF_2 symmetric stretching at 1100 cm^{-1}, and CF_2 asymmetric stretching at 1200 cm^{-1}. None of the bands exhibited any shifts, indicating that changes in chemical structures of the membranes were not detectable, irrespective

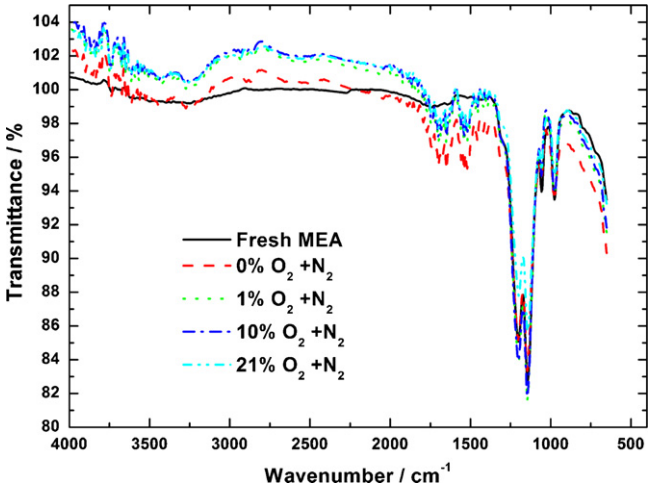

Fig. 10. FT-IR spectra TEM images for the membrane before and after 1200 startup–shutdown cycles employing 0, 1, 10, and 21% O_2 in the purging gas ($N_2 + xO_2$).

of oxygen concentration. Negligible changes in the OCV, hydrogen crossover current density, and chemical structure all support the idea that decay in cell performance is caused by degradation of the cathode rather than the membrane and that the increase in R_{oh} is associated with destruction of the electronic network structure of the cathode. This destruction is probably caused by carbon corrosion and/or a decrease in ionic conductivity of the membrane as a result of penetration and precipitation of Pt particles on the membrane.

4. Conclusions

The effects of residual oxygen partial pressure in a PEMFC stack on the degradation of MEA under reverse current conditions were examined. Increasing the residual oxygen partial pressure from 0 to 21% facilitated the degradation of the cathode and accelerated performance decay. Cathode degradation was revealed by an increase in charge-transfer resistance and a decrease in electrochemical active surface area and could be attributed to corrosion of carbon support and/or dissolution/migration and agglomeration of platinum catalyst. As a new approach to mitigate cathode degradation, suppressing diffusion of ambient air and keeping the residual oxygen partial pressure low were effective at reducing the corrosion of carbon and oxidation/agglomeration of platinum. Therefore, to prevent performance decay during reverse current conditions, oxygen partial pressure in the gas channel of the stack should be kept as low as possible, i.e. by applying a gas-tight air vent to the stack.

Acknowledgements

This work was supported by New and Renewable Energy R&D Program and National R&D Organization for Hydrogen and Fuel Cell under the Korea Ministry of Knowledge Economy as a part of the development of mass production technology for low-cost PEMFC stacks (grant number: 2008-N-FC12-J-02-2-200).

References

[1] B.C.H. Steele, A. Heinzel, Nature 414 (2001) 345–352.
[2] K.E. Martin, J.P. Kopasz, K.W. McMurphy, Fuel Cell Chemistry and Operation (Chapter 1), American Chemical Society, Washington, DC, 2010.
[3] R. Borup, J. Meyers, B. Pivovar, Y.S. Kim, R. Mukundan, N. Garland, D. Myers, M. Wilson, F. Garzon, D. Wood, et al., Chem. Rev. 107 (2007) p.3904.
[4] H. Zhao, A.F. Burke, J. Power Sources 186 (2009) 408.
[5] S. Zhang, X. Yuan, H. Wang, H. Merida, H. Zhu, J. Shen, S. Wu, J. Zhang, Int. J. Hydrogen Energy 34 (2009) 388–404.
[6] T.W. Patterson, R.M. Darling, Electrochem. Solid-State Lett. 9 (2006) A183.
[7] Z.Y. Liu, B.K. Brady, R.N. Carter, B. Litteer, M. Budinski, J.K. Hyun, D.A. Muller, J. Electrochem. Soc. 155 (2008) B979.
[8] H. Tang, Z. Qi, M. Ramani, J.F. Elter, J. Power Sources 158 (2006) 1306.
[9] C.A. Reiser, L. Bregoli, T.W. Patterson, J.S. Yi, J.D. Yang, M.L. Perry, T.D. Jarvi, Electrochem. Solid-State Lett. 8 (2005) A273.
[10] J.H. Kim, E.A. Cho, J.H. Jang, H.J. Kim, T.H. Lim, I.H. Oh, J.J. Ko, S.C. Oh, J. Electrochem. Soc. 156 (2010) B955–B961.
[11] J.H. Kim, E.A. Cho, J.H. Jang, H.J. Kim, T.H. Lim, I.H. Oh, J.J. Ko, S.C. Oh, J. Electrochem. Soc. 157 (2010) B104–B112.
[12] Y.Y. Jo, E.A. Cho, J.H. Kim, T.H. Lim, I.H. Oh, S.K. Kim, H.J. Kim, J.H. Jang, J. Power Sources 196 (2011) 9906–9915.
[13] R.P. O'Hayre, S.W. Cha, W. Colella, F.B. Prinz, Fuel Cell Fundamentals, John Wiley & Sons, New Jersey, 2006.
[14] J.H. Kim, Y.Y. Jo, E.A. Cho, J.H. Jang, H.J. Kim, T.H. Lim, I.H. Oh, J.J. Ko, I.J. Son, J. Electrochem. Soc. 157 (2010) B633–B642.
[15] S.Y. Lee, E.A. Cho, J.H. Lee, H.J. Kim, T.H. Lim, I.H. Oh, J. Won, J. Electrochem. Soc. 154 (2007) B194.
[16] H.J. Kim, S.J. Lim, J.W. Lee, I.G. Min, S.Y. Lee, E.A. Cho, I.H. Oh, J.H. Lee, S.C. Oh, T.W. Lim, et al., J. Power Sources 180 (2008) 814.
[17] J.H. Kim, E.A. Cho, J.H. Jang, H.J. Kim, T.H. Lim, I.H. Oh, J.J. Ko, I.J. Son, J. Electrochem. Soc. 157 (2010) B118–B124.
[18] T.E. Springer, T.A. Zawodzinski, M.S. Wilson, S. Gottesfeld, J. Electrochem. Soc. 143 (1996) 587–599.
[19] E.A. Ticianelli, C.R. Derouin, S. Srinivasan, J. Electroanal. Chem. 251 (1988) 275.
[20] P. Ferreira, G.J. la O', Y. Shao-Horn, D. Morgan, R. Makharia, S.S. Kocha, et al., J. Electrochem. Soc. 152 (2005) A2256–A2271.
[21] J. Zhang, B.A. Litteer, W. Gu, H. Liu, H.A. Gasteiger, J. Electrochem. Soc. 154 (2007) B1006–B1011.
[22] F. Rong, C. Huang, Z-S. Liu, D. Song, Q. Wang, J. Power Sources 175 (2008) 699–711.
[23] Z. Liang, W. Chen, J. Liu, S. Wang, Z. Zhou, W. Li, G. Sun, Q. Xin, J. Membr. Sci. 233 (2004) 39–44.